TÜBİTAK

Turkish Journal of Mathematics

http://journals.tubitak.gov.tr/math/

Research Article

Turk J Math
(2019) 43: 112 – 125
© TÜBİTAK
doi:10.3906/mat-1804-55

Quartic trigonometric B-spline algorithm for numerical solution of the regularized long wave equation

Dursun IRK, Pınar KESKİN YILDIZ, Melis ZORŞAHİN GÖRGÜLÜ*
Department of Mathematics and Computer Science, Faculty of Science and Letters, Eskişehir Osmangazi University, Eskişehir, Turkey

Received: 17.04.2018 • **Accepted/Published Online:** 24.10.2018 • **Final Version:** 18.01.2019

Abstract: In this paper, an application of the quartic trigonometric B-spline finite element method is used to solve the regularized long wave equation numerically. This approach involves a Galerkin method based on the quartic trigonometric B-spline function in space discretization together with second and fourth order schemes in time discretization. The accuracy of the proposed methods are demonstrated by test problems and numerical results are compared with the exact solution and some previous results.

Key words: Galerkin method, quartic trigonometric B-spline, regularized long wave equation, multistep methods

1. Introduction

The regularized long wave (RLW) equation is one of the model nonlinear evolution equations, which was first introduced by Peregrine [22] to explain the development of the undular bore. The RLW equation has also been used to describe many physical phenomena in various areas of science such as shallow water waves, ion-acoustic waves in plasma, etc. Analytical solutions of nonlinear partial differential equations (PDEs) are generally not available, so numerical solutions of these equations are very important in applied science. Therefore, various numerical methods of solving the RLW equation have been proposed so far, such as finite difference and finite element methods [4, 11, 12, 16, 18, 21, 28].

Splines are a class of piecewise polynomials that have continuity depending on the degrees of the polynomials. Since they have important geometric properties and lower computational cost, the bases of splines known as B-splines are widely used for numerical methods. In 1964 Schoenberg introduced trigonometric spline functions and proved the existence of locally supported trigonometric spline and B-spline functions [25]. Koch constructed a class of multivariate trigonometric B-splines from the multivariate polynomial ones [15]. The derivation and some properties of the trigonometric B-splines were investigated in studies [17, 26]. Nicolis presented a numerical method for solving ordinary differential equations with quadratic trigonometric splines [19]. The linear two-point boundary value problems of order two were solved using the cubic trigonometric B-spline interpolation method in [10]. Abbas et al. proposed a collocation finite difference scheme based on cubic trigonometric B-spline for the numerical solution of a one-dimensional hyperbolic equation (wave equation) with the nonlocal conservation condition [1]. Burgers' equation was solved by the collocation method using the

*Correspondence: mzorsahin@ogu.edu.tr
2010 *AMS Mathematics Subject Classification:* 65M70, 76B25, 65D07

cubic trigonometric B-spline and the subdomain Galerkin method using the quadratic trigonometric B-spline, respectively, in [2, 5]. The cubic and quadratic trigonometric B-spline Galerkin finite element methods were proposed for the numerical solution of the RLW equation by Irk and Keskin [13, 14]. Some researchers showed that the accuracy of the numerical solutions of PDEs are improved if the Galerkin finite element method is used for space discretization together with B-spline functions. However, as far as we know, no work has been found for the numerical solution of any equation using the quartic trigonometric B-spline Galerkin method.

We will consider the RLW equation in the following form:

$$u_t + u_x + \varepsilon u u_x - \mu u_{xxt} = 0, \tag{1}$$

with the boundary conditions $u \to 0$ as $x \to \pm\infty$, where u represents dimensionless surface elevation, ε and μ are positive parameters, and subscripts x and t denote distance and time, respectively.

To apply the numerical method, the distance variable x of the problem is restricted over a finite interval $[a, b]$. In addition, the space interval must be chosen as large as possible to fit the boundary condition $u \to 0$ as $x \to \pm\infty$. In this study boundary conditions will be selected over the space region as

$$\begin{aligned} u(a,t) &= \alpha_1 \\ u(b,t) &= \alpha_2, \qquad t \in (0,T] \\ u_x(a,t) &= 0, \\ u_x(b,t) &= 0 \end{aligned} \tag{2}$$

and the initial condition

$$u(x,0) = f(x) \tag{3}$$

will be chosen in the numerical experiments section.

In this paper, we have set up an algorithm for the numerical solutions of the RLW equation by using the quartic trigonometric B-spline Galerkin method based on the second and fourth order time discretization method. In Section 2, the proposed method is presented. In Section 3, the propagation of a solitary wave, the interaction of two positive solitary waves, and the wave generation test problems are treated for the efficiency and the accuracy of the method. The results obtained are compared with exact results and also other numerical results given in the literature in terms of norm L_∞ and conservative quantities.

2. Quartic trigonometric B-spline Galerkin method

The exact solutions of the unknown functions at the grid points are expressed as follows:

$$u(x_m, t_n) = u_m^n, \ m = 0, 1, \ldots, N; \qquad n = 0, 1, 2, \ldots$$

where $x_m = a + mh$, $t_n = n\Delta t$, and the notation U_m^n is used to represent the numerical value of u_m^n.

2.1. Time discretization

We rewrite the RLW equation in the following form:

$$v_t = (u - \mu u_{xx})_t = -(u_x + \varepsilon u u_x). \tag{4}$$

The time discretization of Eq. (4) is carried out using the following one-step and two-step methods:

$$v^{n+1} = v^n + \frac{\Delta t}{2}\left((v_t)^{n+1} + (v_t)^n\right) + \mathcal{O}(\Delta t^3), \tag{5}$$

$$v^{n+1} = v^{n-1} + \frac{\Delta t}{3}\left((v_t)^{n+1} + 4(v_t)^n + (v_t)^{n-1}\right) + \mathcal{O}(\Delta t^5). \tag{6}$$

The second method is typically more accurate than the first method because its order is bigger than that of the first method. The general form of the above methods can be written as follows:

$$v^{n+1} = \theta_1 v^n + \theta_2 v^{n-1} + \theta_3 (v_t)^{n+1} + \theta_4 (v_t)^n + \theta_5 (v_t)^{n-1}. \tag{7}$$

If $\theta_1 = 1,\ \theta_2 = 0,\ \theta_3 = \theta_4 = \Delta t/2,\ \theta_5 = 0,$ the method is of order 2 and is called the Crank–Nicolson method (M1), and if $\theta_1 = 0,\ \theta_2 = 1,\ \theta_3 = \Delta t/3,\ \theta_4 = 4\Delta t/3,\ \theta_5 = \Delta t/3,$ the method is of order 4 and is called Simpson's method (M2). Using (7) given above in (4) leads to

$$\begin{array}{l} u^{n+1} - \mu u_{xx}^{n+1} + \theta_3\left(u_x^{n+1} + \varepsilon u^{n+1} u_x^{n+1}\right) = \\ \theta_1\left(u^n - \mu u_{xx}^n\right) - \theta_4\left(u_x^n + \varepsilon u^n u_x^n\right) + \\ \theta_2\left(u^{n-1} - \mu u_{xx}^{n-1}\right) - \theta_5\left(u_x^{n-1} + \varepsilon u^{n-1} u_x^{n-1}\right). \end{array} \tag{8}$$

2.2. Space discretization

We subdivide the solution domain $[a, b]$ into uniformly spaced finite elements that have length of h by knots

$$a = x_0 < x_1 < \ldots < x_{N-1} < x_N = b.$$

The quartic trigonometric B-spline functions at these knots are obtained using the recurrence relation given [17, 26] as

$$T_m(x) = \frac{1}{\theta}\begin{cases} \rho^4(x_{m-2}), & , x_{m-2} \le x < x_{m-1} \\ \begin{array}{l} -\rho^3(x_{m-2})\rho(x_m) - \rho^2(x_{m-2})\rho(x_{m+1})\rho(x_{m-1}) \\ -\rho(x_{m-2})\rho(x_{m+2})\rho^2(x_{m-1}) - \rho(x_{m+3})\rho^3(x_{m-1}), \end{array} & , x_{m-1} \le x < x_m \\ \begin{array}{l} \rho^2(x_{m-2})\rho^2(x_{m+1}) + \rho(x_{m-2})\rho(x_{m+2})\rho(x_{m-1})\rho(x_{m+1}) \\ +\rho(x_{m-2})\rho^2(x_{m+2})\rho(x_m) + \rho(x_{m+3})\rho^2(x_{m-1})\rho(x_{m+1}) \\ +\rho(x_{m+3})\rho(x_{m-1})\rho(x_{m+2})\rho(x_m) + \rho^2(x_{m+3})\rho^2(x_m), \end{array} & , x_m \le x < x_{m+1} \\ \begin{array}{l} -\rho(x_{m-2})\rho^3(x_{m+2}) - \rho(x_{m+3})\rho(x_{m-1})\rho^2(x_{m+2}) \\ -\rho^2(x_{m+3})\rho(x_m)\rho(x_{m+2}) - \rho^3(x_{m+3})\rho(x_{m+1}), \end{array} & , x_{m+1} \le x < x_{m+2} \\ \rho^4(x_{m+3}), & , x_{m+2} \le x < x_{m+3} \\ 0, & \text{otherwise} \end{cases} \tag{9}$$

where

$$\theta = \sin\left(\frac{h}{2}\right)\sin(h)\sin\left(\frac{3h}{2}\right)\sin(2h),$$

$$\rho(x_m) = \sin\left(\frac{x - x_m}{2}\right).$$

The set of quartic trigonometric B-splines $T_m(x)$, $m=-2,\ldots,N+1$, forms a basis over the problem domain $[a,b]$. Thus, the global approximate solution to the analytical solution for Eq. (1) can be defined in terms of the quartic trigonometric B-splines as

$$u(x,t)\approx U(x,t)=\sum_{m=-2}^{N+1}T_m(x)\delta_m(t), \tag{10}$$

where the values of $\delta_m(t)$ are time-dependent parameters that will be determined from the boundary and quartic trigonometric B-spline Galerkin form of Eq. (1). Since each quartic trigonometric B-spline covers five finite elements, each typical finite element $[x_m,x_{m+1}]$ is covered by five quartic trigonometric B-spline functions. Then we have

$$U(x_m,t)=\sum_{j=m-2}^{m+2}T_j(x_m)\delta_j(t). \tag{11}$$

Approximation of the nodal values U_m and the three principal space derivatives over the element $[x_m,x_{m+1}]$ can be obtained in terms of the parameters δ_m using (9) in (11) as

$$\begin{aligned}
U_m &= a_1\delta_{m-2}+a_2\delta_{m-1}+a_2\delta_m+a_1\delta_{m+1},\\
\frac{\partial U_m}{\partial x} &= b_1\delta_{m-2}+b_2\delta_{m-1}-b_2\delta_m-b_1\delta_{m+1},\\
\frac{\partial^2 U_m}{\partial x^2} &= c_1\delta_{m-2}-c_1\delta_{m-1}-c_1\delta_m+c_1\delta_{m+1},\\
\frac{\partial^3 U_m}{\partial x^3} &= d_1\delta_{m-2}+d_2\delta_{m-1}-d_2\delta_m-d_1\delta_{m+1},
\end{aligned} \tag{12}$$

where

$$a_1=\frac{\sin^4\left(\frac{h}{2}\right)}{\theta},\qquad a_2=\frac{\sin^4\left(\frac{h}{2}\right)\left(12\cos^2\left(\frac{h}{2}\right)-1\right)}{\theta},$$

$$b_1=-\frac{2\sin^3\left(\frac{h}{2}\right)\cos\left(\frac{h}{2}\right)}{\theta},\qquad b_2=-\frac{2\sin^3\left(\frac{h}{2}\right)\cos\left(\frac{h}{2}\right)\left(4\cos^2\left(\frac{h}{2}\right)-1\right)}{\theta},$$

$$c_1=\frac{\sin^2\left(\frac{h}{2}\right)\left(4\cos^2\left(\frac{h}{2}\right)-1\right)}{\theta},\qquad d_1=-\frac{\sin\left(\frac{h}{2}\right)\cos\left(\frac{h}{2}\right)\left(8\cos^2\left(\frac{h}{2}\right)-5\right)}{\theta},$$

$$d_2=\frac{\sin\left(\frac{h}{2}\right)\cos\left(\frac{h}{2}\right)\left(4\cos^2\left(\frac{h}{2}\right)-1\right)^2}{\theta}.$$

A typical finite interval $[x_m,x_{m+1}]$ is transformed into the interval $[0,h]$ by the local coordinate transformation $\xi=x-x_m$, $0<\xi<h$. The quartic trigonometric B-spline shape functions (9) in terms of ξ over $[0,h]$ can be

written as

$$
\begin{aligned}
T_{m-2}(\xi) &= \frac{\sin^4\left(\frac{\xi-h}{2}\right)}{\theta} \\
T_{m-1}(\xi) &= \frac{1}{\theta}\left[\sin\left(\frac{\xi+3h}{2}\right)\sin^3\left(\frac{h-\xi}{2}\right)+\sin\left(\frac{2h-\xi}{2}\right)\sin\left(\frac{\xi+2h}{2}\right)\sin^2\left(\frac{\xi-h}{2}\right)\right. \\
&\quad \left.+\sin^2\left(\frac{\xi-2h}{2}\right)\sin\left(\frac{\xi+h}{2}\right)\sin\left(\frac{h-\xi}{2}\right)+\sin^3\left(\frac{2h-\xi}{2}\right)\sin\left(\frac{\xi}{2}\right)\right] \\
T_m(\xi) &= \frac{1}{\theta}\left[\sin^2\left(\frac{\xi+2h}{2}\right)\sin^2\left(\frac{\xi-h}{2}\right)\right. \\
&\quad +\sin\left(\frac{\xi+2h}{2}\right)\sin\left(\frac{\xi-2h}{2}\right)\sin\left(\frac{\xi+h}{2}\right)\sin\left(\frac{\xi-h}{2}\right) \\
&\quad +\sin\left(\frac{\xi+2h}{2}\right)\sin^2\left(\frac{\xi-2h}{2}\right)\sin\left(\frac{\xi}{2}\right) \\
&\quad +\sin\left(\frac{\xi-3h}{2}\right)\sin^2\left(\frac{\xi+h}{2}\right)\sin\left(\frac{\xi-h}{2}\right) \\
&\quad +\sin\left(\frac{\xi-3h}{2}\right)\sin\left(\frac{\xi+h}{2}\right)\sin\left(\frac{\xi-2h}{2}\right)\sin\left(\frac{\xi}{2}\right) \\
&\quad \left.+\sin^2\left(\frac{\xi-3h}{2}\right)\sin^2\left(\frac{\xi}{2}\right)\right] \\
T_{m+1}(\xi) &= \frac{1}{\theta}\left[\sin^3\left(\frac{\xi+h}{2}\right)\sin\left(\frac{h-\xi}{2}\right)\right. \\
&\quad +\sin^2\left(\frac{\xi+h}{2}\right)\sin\left(\frac{2h-\xi}{2}\right)\sin\left(\frac{\xi}{2}\right) \\
&\quad \left.+\sin\left(\frac{\xi+h}{2}\right)\sin\left(\frac{3h-\xi}{2}\right)\sin^2\left(\frac{\xi}{2}\right)+\sin\left(\frac{4h-\xi}{2}\right)\sin^3\left(\frac{\xi}{2}\right)\right] \\
T_{m+2}(\xi) &= \frac{\sin^4\left(\frac{\xi}{2}\right)}{\theta}.
\end{aligned}
\tag{13}
$$

Thus, the approximation to the exact solution $u(x,t)$ can be expressed over the element $[0,h]$ as

$$
U(\xi,t)=\sum_{j=m-2}^{m+2} T_j(\xi)\delta_j(t),\ m=0,\ldots,N-1, \tag{14}
$$

where δ_j and T_j are element parameters and element shape functions, respectively.

Applying the Galerkin method to Eq. (8), we have the integral equation

$$\begin{aligned}
&\int_a^b W(x)\left[U^{n+1}+\theta_3\left(\left(U_x\right)^{n+1}+\varepsilon U^{n+1}\left(U_x\right)^{n+1}\right)-\mu\left(U_{xx}\right)^{n+1}\right]dx=\\
&\int_a^b W(x)\left[\theta_1\left(U^n-\mu\left(U_{xx}\right)^n\right)-\theta_4\left(\left(U_x\right)^n+\varepsilon U^n\left(U_x\right)^n\right)\right]dx+\\
&\int_a^b W(x)\left[\theta_2\left(U^{n-1}-\mu\left(U_{xx}\right)^{n-1}\right)-\theta_5\left(\left(U_x\right)^{n-1}+\varepsilon U^{n-1}\left(U_x\right)^{n-1}\right)\right]dx,
\end{aligned}\tag{15}$$

where $W(x)$ is a weight function.

In the above equation, taking the weight function $W(x)$ as the quartic trigonometric B-spline T_m and using element trial function (14), a fully discrete approximation is obtained over the element $[0,h]$ as

$$\begin{aligned}
&\sum_{j=m-2}^{m+2}\left\{\left(\int_0^h T_iT_jd\xi\right)\delta_j^{n+1}-\mu\left(\int_0^h T_iT_j''d\xi\right)\delta_j^{n+1}+\theta_3\left(\int_0^h T_iT_j'd\xi\right)\delta_j^{n+1}\right.\\
&\left.+\theta_3\varepsilon\sum_{k=m-2}^{m+2}\left(\int_0^h T_iT_k\left(\delta_k^{n+1}\right)T_j'd\xi\right)\delta_j^{n+1}\right\}-\sum_{j=m-2}^{m+2}\left\{\theta_1\left(\int_0^h T_iT_jd\xi\right)\delta_j^n\right.\\
&\left.-\mu\theta_1\left(\int_0^h T_iT_j''d\xi\right)\delta_j^n-\theta_4\left(\int_0^h T_iT_j'd\xi\right)\delta_j^n-\theta_4\varepsilon\sum_{k=m-2}^{m+2}\left(\int_0^h T_iT_k\left(\delta_k^n\right)T_j'd\xi\right)\delta_j^n\right\}\\
&-\sum_{j=m-2}^{m+2}\left\{\theta_2\left(\int_0^h T_iT_jd\xi\right)\delta_j^{n-1}-\mu\theta_2\left(\int_0^h T_iT_j''d\xi\right)\delta_j^{n-1}-\theta_5\left(\int_0^h T_iT_j'd\xi\right)\delta_j^{n-1}\right.\\
&\left.-\theta_5\varepsilon\sum_{k=m-2}^{m+2}\left(\int_0^h T_iT_k\left(\delta_k^{n-1}\right)T_j'd\xi\right)\delta_j^{n-1}\right\},
\end{aligned}\tag{16}$$

where i also takes the values $m-2, m-1, m, m+1, m+2$. The above equation can be expressed in matrix form as

$$\begin{aligned}
&\left[\mathbf{A}^e-\mu\mathbf{D}^e+\theta_3\left(\mathbf{B}^e+\varepsilon\mathbf{C}^e\left(\boldsymbol{\delta}^e\right)^{n+1}\right)\right]\left(\boldsymbol{\delta}^e\right)^{n+1}\\
&-\left[\theta_1\left(\mathbf{A}^e-\mu\mathbf{D}^e\right)-\theta_4\left(\mathbf{B}^e+\varepsilon\mathbf{C}^e\left(\boldsymbol{\delta}^e\right)^n\right)\right]\left(\boldsymbol{\delta}^e\right)^n\\
&-\left[\theta_2\left(\mathbf{A}^e-\mu\mathbf{D}^e\right)-\theta_5\left(\mathbf{B}^e+\varepsilon\mathbf{C}^e\left(\boldsymbol{\delta}^e\right)^{n-1}\right)\right]\left(\boldsymbol{\delta}^e\right)^{n-1},
\end{aligned}\tag{17}$$

where $\left(\boldsymbol{\delta}^e\right)^{n+1}=\left(\delta_{m-2}^{n+1},\ldots,\delta_{m+2}^{n+1}\right)^T$.

$\mathbf{A}^e, \mathbf{B}^e$, and $\mathbf{D}^e$ are the element matrices with dimensions 5×5; $\mathbf{C}^e$ is the element matrix with dimension $5\times5\times5$; and these element matrices are denoted by

$$\begin{aligned}
A_{ij}^e &= \int_0^h T_iT_jd\xi,\quad B_{ij}^e=\int_0^h T_iT_j'd\xi,\\
C_{ij}^e\left(\boldsymbol{\delta}^e\right)^{n+1} &= \int_0^h T_iT_k\boldsymbol{\delta}_k^{n+1}T_j'd\xi,\quad D_{ij}^e=\int_0^h T_iT_j''d\xi.
\end{aligned}$$

In the above notation, $\mathbf{A}^e, \mathbf{B}^e$, and $\mathbf{D}^e$ are independent of the parameters $\boldsymbol{\delta}^e$ and $\mathbf{C}^e$ depends on the parameters $\boldsymbol{\delta}^e$. The nonlinear matrix equation is produced by assembling the systems of (17) over all elements

$$\begin{aligned}
\left[\mathbf{A}-\mu\mathbf{D}+\theta_3\left(\mathbf{B}+\varepsilon\mathbf{C}\boldsymbol{\delta}^{n+1}\right)\right]\boldsymbol{\delta}^{n+1}&=\left[\theta_1\left(\mathbf{A}-\mu\mathbf{D}\right)-\theta_4\left(\mathbf{B}+\varepsilon\mathbf{C}\boldsymbol{\delta}^n\right)\right]\boldsymbol{\delta}^n\\
&+\left[\theta_2\left(\mathbf{A}-\mu\mathbf{D}\right)-\theta_5\left(\mathbf{B}+\varepsilon\mathbf{C}\boldsymbol{\delta}^{n-1}\right)\right]\boldsymbol{\delta}^{n-1},
\end{aligned}\tag{18}$$

where $\boldsymbol{\delta}=(\delta_{-2},,\ldots,\delta_{N+1})^T$ and $\mathbf{A},\mathbf{B},\mathbf{C}$, and $\mathbf{D}$ are derived from the corresponding element matrices $\mathbf{A}^e,\mathbf{B}^e,\mathbf{C}^e$, and $\mathbf{D}^e$.

The set of Eq. (18) consists of $(N+4)$ equations with $(N+4)$ unknown parameters $(\delta_{-2},\ldots,\delta_{N+1})$. The initial vector $\delta^0=(\delta^0_{-},\ldots,\delta^0_{N+1})$ can be found with the help of the boundary and initial conditions and then $\delta^1=(\delta^1_{-2},\ldots,\delta^1_{N+1})$ unknown vector is obtained using M1. Therefore, $\delta^{n+1}(n=1,2,\ldots)$ unknown vectors can be found repeatedly by solving the recurrence relation (18) using two precious δ^n and δ^{n-1} unknown vectors. Note that since system (18) is an implicit system, an inner iteration algorithm is employed at all time steps.

3. Numerical tests

The three invariants of the motion for the RLW equation corresponding to mass, momentum, and energy, respectively, are given by [20] as

$$I_1=\int_{-\infty}^{\infty} u dx,$$
$$I_2=\int_{-\infty}^{\infty}(u^2+\mu(u_x)^2)dx, \tag{19}$$
$$I_3=\int_{-\infty}^{\infty}\left(u^3+3u^2\right)dx.$$

These integrals (19) are calculated approximately with the trapezoidal rule for the space interval $[a,b]$ at all time steps. We present three numerical test problems including motion of a single solitary wave, interaction of two solitary waves, and wave generation to exhibit the efficiency of the method. For the first test problem, accuracy of the method is calculated using the following error norm;

$$L_\infty=\max_m|u_m-U_m|, \tag{20}$$

and the order of convergence is computed by

$$\text{order}=\frac{\log\dfrac{(L_\infty)_{\Delta t_m}}{(L_\infty)_{\Delta t_{m+1}}}}{\log\dfrac{\Delta t_m}{\Delta t_{m+1}}}, \tag{21}$$

where $(L_\infty)_{\Delta t_m}$ is the error norm L_∞ with time step Δt_m.

3.1. Motion of single solitary wave

The theoretical solution of the RLW equation,

$$u(x,t)=3c\,\text{sech}^2(k[x-\tilde{x}_0-vt]), \tag{22}$$

represents a single solitary wave. Here $3c$ depicts magnitude, the wave velocity is $v=1+\varepsilon c$, peak position of the initially centered wave is $\tilde{x}_0$, and $k=\sqrt{\dfrac{\varepsilon c}{4\mu v}}$. The boundary conditions are chosen as $\alpha_1=\alpha_2=0$. By

taking $t = 0$ in the analytical solution (22), the initial condition can be obtained as

$$u(x,0) = 3c\text{sech}^2(k[x - \tilde{x}_0]). \tag{23}$$

In this test problem, a single solitary wave propagates towards the right across the interval $-80 \leq x \leq 120$ in the time period $0 \leq t \leq 20$ with the parameters $\varepsilon = \mu = 1$, $\tilde{x}_0 = 0$, and the amplitude $3c = 0.3$. Using these parameters and $h = \Delta t = 0.1$, the initial and numerical solutions at various times are illustrated in Figure 1 for M2. According to the figure we can say that the solitary wave remains in its initial form during the running time. Using initial condition (23), analytical values of invariants can be determined as

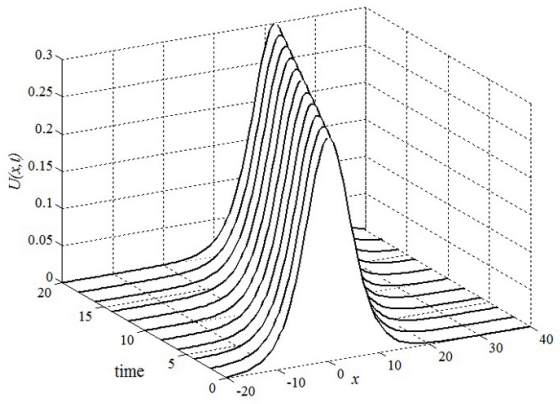

Figure 1. $U(x,t)$ at various times with $h = \Delta t = 0.1$.

$$I_1 = \frac{6c}{k}, \quad I_2 = \frac{12c^2}{k} + \frac{48kc^2\mu}{5}, \quad I_3 = \frac{36c^2}{k}\left(1 + \frac{4c}{5}\right).$$

The algorithm is run up to time $t = 20$ with constant space and various time steps. Error norm L_∞ and conservation invariants are presented in Table 1 with $c = 0.1$ for each proposed method. According to the table, while equal space and time steps are decreased from 1 to 0.05, all of the error norms L_∞ are decreased for each proposed methods. The numerical values of the conservation invariants also remain almost the same as their analytical values, which are given in Table 1. When we compare the performance of the algorithms by their orders of convergence, it can be seen that M1 and M2 have a quadratic and quartic order of convergence, respectively.

The distribution of the absolute error (analytical – numerical) at time $t = 20$ is demonstrated in Figure 2 for each proposed method. As seen from the figures, the maximum error is observed at the middle of the space interval, and this result is also compatible with Table 1.

The obtained error norm L_∞ and conservation invariants are presented in Table 2 for a different problem domain and our results are compared with previous studies. According to the table, our results, especially those obtained by M2, have smaller error than other ones given in the table. Also, it can be clearly seen that the accuracy of the approach is increased by the application of the fourth order time discretization method.

Table 1. Error norms L_∞ and invariants for a single solitary wave at time $t = 20$ with $c = 0.1$, $-80 \le x \le 120$.

M1					
$\Delta t = h$	L_∞	Order	I_1	I_2	I_3
2	2.75×10^{-2}	1.80	3.9797178322	0.8168587519	2.5813636888
1	7.91×10^{-3}	1.90	3.9799236234	0.8107010745	2.5791390301
0.5	2.13×10^{-3}	1.97	3.9799462452	0.8104762119	2.5790146079
0.2	3.48×10^{-4}	1.99	3.9799495176	0.8104627943	2.5790074662
0.1	8.75×10^{-5}	2.00	3.9799497193	0.8104625078	2.5790074216
0.05	2.19×10^{-5}	2.00	3.9799497447	0.8104624944	2.5790074339
0.02	3.51×10^{-6}		3.9799497481	0.8104624942	2.5790074367
M2					
2	1.49×10^{-3}	3.40	3.9800117236	0.8161367475	2.5793314701
1	1.42×10^{-4}	4.02	3.9799455274	0.8106353995	2.5790088514
0.5	8.72×10^{-6}	4.04	3.9799492107	0.8104719568	2.5790070078
0.2	2.16×10^{-7}	4.09	3.9799497137	0.8104627210	2.5790073990
0.1	1.27×10^{-8}	4.19	3.9799497440	0.8104625075	2.5790074319
0.05	6.96×10^{-10}	3.76	3.9799497478	0.8104624950	2.5790074363
0.02	2.22×10^{-11}		3.9799497483	0.8104624942	2.5790074369
Exact	0		3.9799497484	0.8104624942	2.5790074370

Table 2. Solitary wave amplitude$= 0.3$ at $t = 20$ with $h = 0.125, \Delta t = 0.1$.

	$L_\infty \times 10^5$	I_1	I_2	I_3
M1$(-80 \le x \le 120)$	8.752	3.9799497	0.8104625	2.5790074
M2$(-80 \le x \le 120)$	0.001	3.9799497	0.8104625	2.5790074
M1$(-40 \le x \le 60)$	8.752	3.9798832	0.8104625	2.5790074
M2$(-40 \le x \le 60)$	1.268	3.9798832	0.8104625	2.5790074
[27]$(-40 \le x \le 60)$	25.398	3.97989	0.80925	2.57501
[27]$(-80 \le x \le 120, h = 0.2)$	14.240	3.97829	0.80983	2.57692
[8]$(-40 \le x \le 60)$	8.6	3.97988	0.810465	2.57901
[6]QBGM1$(-40 \le x \le 60)$	7.3	3.97988	0.81046	2.57900
[6]QBGM2$(-40 \le x \le 60)$	12.8	3.97988	0.81046	2.57900
[23]$(-40 \le x \le 60)$	7.344	3.9798879	0.8104622	2.5790063
[7]$(-40 \le x \le 60)$	19.8	3.98206	0.811164	2.58133
[21]$(-40 \le x \le 60)$	11.5	3.97988	0.81046	2.57900
[14]CN1$(-80 \le x \le 100)$	8.78896	3.9799498	0.8104273	2.5790075
[14]CN2$(-80 \le x \le 100)$	8.79019	3.9799498	0.8104273	2.5790075
[14]AM1$(-80 \le x \le 100)$	0.20615	3.9799498	0.8104625	2.5790074
[14]AM2$(-80 \le x \le 100)$	0.21010	3.9799498	0.8104298	2.5790159
Exact		3.9799497	0.8104625	2.5790074

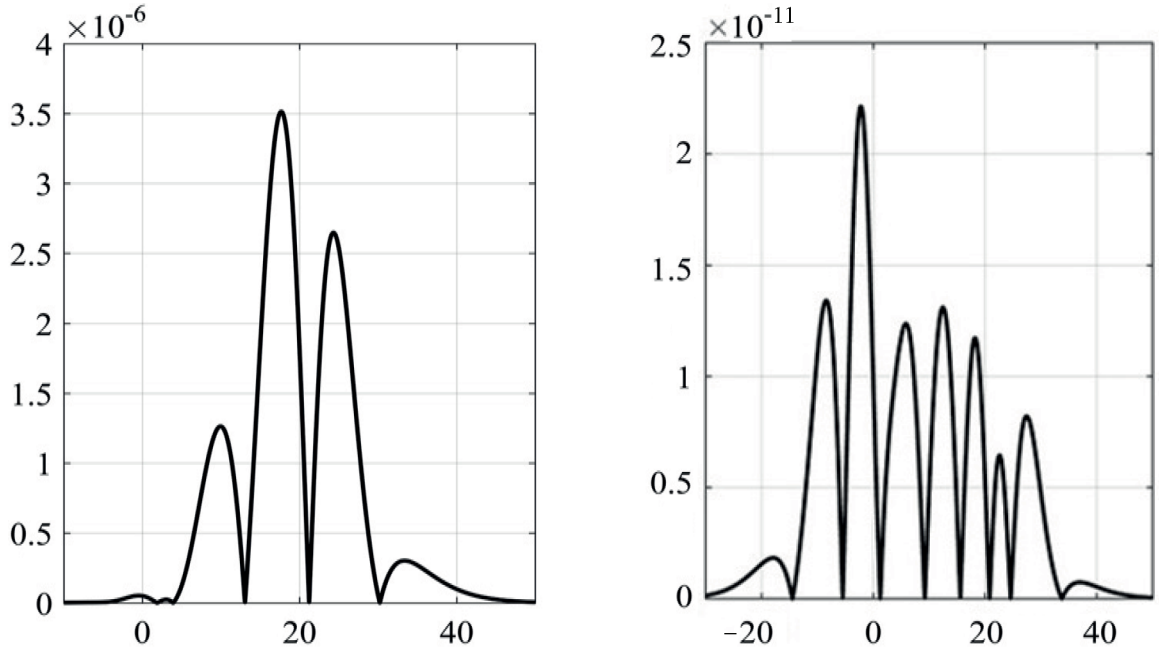

Figure 2. Absolute error with $h = \Delta t = 0.02$ for the proposed methods.

3.2. Interaction of two solitary waves

The initial condition of the interaction of two solitary waves is expressed in the following form:

$$u(x,0) = 3c_1 \mathrm{sech}^2(k_1[x-\tilde{x}_1]) + 3c_2 \mathrm{sech}^2(k_2[x-\tilde{x}_2]), \tag{24}$$

where $k_i = \sqrt{\dfrac{\varepsilon c_i}{4\mu\,(1+\varepsilon c_i)}}, i = 1,2$.

For the computational work and the comparison with earlier studies, we choose the parameters $\varepsilon = \mu = 1$, $c_1 = 1.5$, $c_2 = 0.5$, $\tilde{x}_1 = 20$, and $\tilde{x}_2 = 50$ over the space interval $0 \le x \le 180$ with the boundary conditions $\alpha_1 = \alpha_2 = 0$. First of all, two well separated solitary waves of magnitudes 4.5 and 1.5 are obtained with these parameters. Peak positions of these solitary waves are located at $x = 20$ and 50, respectively. Calculations are run up to time $t = 50$ with space and time step $h = \Delta t = 0.1$. Numerical solutions of $U(x,t)$ for M2 are plotted for the visual views of the solutions at various times in Figure 3. According to the figure, the larger wave is placed to the left of the smaller wave. Later, both waves move to the right over the interval and the larger wave catches up to the smaller one. The nonlinear interaction takes places at about time $t = 25$, and after the interaction, two solitary waves start to resume their original shapes. The analytical invariants can be calculated as

$$I_1 = \frac{6c_1}{k_1} + \frac{6c_2}{k_2}, \quad I_2 = \frac{12c_1^2}{k_1} + \frac{48k_1c_1^2\mu}{5} + \frac{12c_2^2}{k_2} + \frac{48k_2c_2^2\mu}{5},$$
$$I_3 = \frac{36c_1^2}{k_1}\left(1 + \frac{4c_1}{5}\right) + \frac{36c_2^2}{k_2}\left(1 + \frac{4c_2}{5}\right).$$

In the Table 3, the conservation invariants are compared for M1 and M2 with equal space and time steps. The table indicates that the changes of the invariants are fairly small for M2.

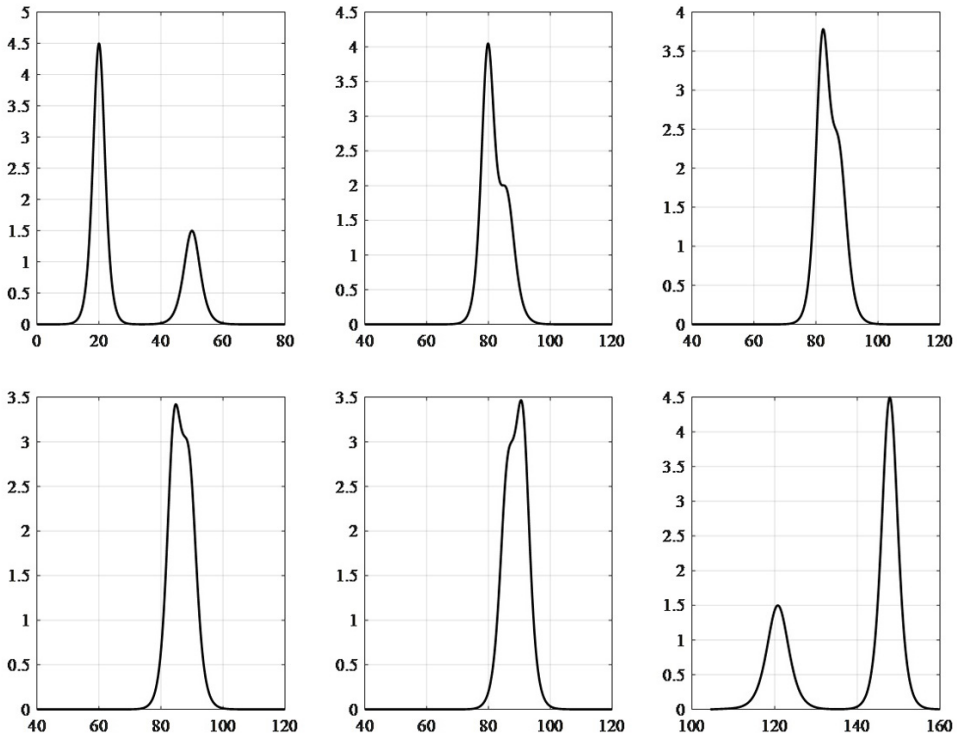

Figure 3. Interaction of two solitary waves for M2 at various times with $h = \Delta t = 0.1$.

Table 3. Invariants for interaction of two solitary waves.

$h = \Delta t$	M1			M2		
	I_1	I_2	I_3			
0.20	33.1031	86.5961	484.5780	33.5408	88.7070	500.3422
0.10	33.5551	88.7915	500.9674	33.6187	89.1067	503.3263
0.05	33.6205	89.1162	503.3970	33.6288	89.1572	503.7041
0.02	33.6296	89.1612	503.7349	33.6301	89.1640	503.7548
Exact	33.6302	89.1645	503.7581	33.6302	89.1645	503.7581

Table 4. Amplitudes of larger and smaller waves at $t = 50$.

$h = \Delta t$	M1		M2	
	Smaller wave	Larger wave	Smaller wave	Larger wave
0.2	1.49358	4.37404	1.49829	4.48577
0.10	1.49705	4.47638	1.49831	4.49671
0.05	1.49809	4.49545	1.49837	4.49966
0.02	1.49839	4.49947	1.49841	4.49997
exact	1.5	4.5	1.5	4.5

In Table 4, amplitudes of larger and smaller waves at $t = 50$ for both methods are given. While equal space and time steps are decreased from 0.2 to 0.02, the numerical values of the amplitudes for both proposed methods are getting close to the exact values of the amplitudes.

3.3. Wave generation

The wave marker boundary condition

$$u(a,t) = \alpha_1 = \begin{cases} U_0 \dfrac{t}{\tau}, & 0 \le t \le \tau, \\ U_0, & \tau < t < t_0 - \tau, \\ U_0 \dfrac{t_0 - t}{\tau}, & t_0 - \tau \le t \le t_0, \\ 0, & \text{otherwise} \end{cases}$$

and $u(b,t) = \alpha_2 = 0$ are used to generate waves with the RLW equation.

By choosing the parameters as $U_0 = 2$, $\Delta t = 0.1$, $h = 0.4$, $t_0 = 20$, and $\tau = 0.3$ over the region $0 \le x \le 260$, the amplitudes of the solitary waves and the conservation constants at time $t = 100$ are listed in Table 5 for comparison of both of the proposed methods with earlier works. Generation of the solitary waves is depicted in Figure 4 for M2. It can be said that five solitary waves are produced by the left-side boundary condition's effect.

Table 5. Solitary wave amplitude with $U_0 = 2$, $h = 0.4$, $\Delta t = 0.1$, and period of forcing $0 \le t_0 \le 20$, $0 \le x \le 260$.

Time	1	2	3	4	5	I_1	I_2	I_3
100 for M1	3.75	3.50	3.06	2.34	1.08	78.5000	174.7550	885.4053
100 for M2	3.74	3.51	3.06	2.34	1.09	78.6110	175.4408	889.2835
100 Ref. [29]	3.68	3.47	3.03	2.32	1.07	78.2589	172.0094	867.7610
100 Ref. [9]	3.76	3.52	3.06	2.33	1.07			
100 Ref. [24]	3.77	3.52	3.08	2.38	1.18			
100 Ref. [3]	3.76	3.51	3.07	2.31	0.98			

4. Conclusion

The Galerkin finite element method based on quartic trigonometric B-splines as weight and trial functions for space discretization and Crank–Nicolson and Simpson's methods for time discretization have been proposed to get a numerical solution to the RLW equation. According to the time discretization, the first method is of order 2 and the second method is of order 4. The performances of the proposed methods have been examined well by studying three test problems including the propagation of a single solitary wave, interaction of solitary waves, and wave generation. Comparing all the proposed methods with previous studies, M2 gives accurate and reliable results for the numerical solution of the RLW equation.

Acknowledgment

This work was supported by the Scientific Research Council of Eskişehir Osmangazi University under Project No. 2014-581.

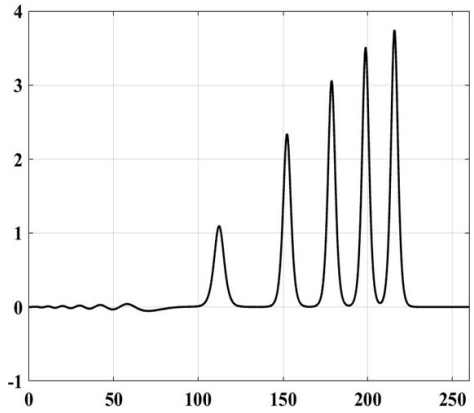

Figure 4. Solitary wave produced by boundary forcing of duration $t_0 = 20$ and amplitude $U_0 = 2$ at time $t = 100$, $h = 0.4$, $\Delta t = 0.1$.

References

[1] Abbas M, Majid AA, Ismail AIM, Rashid A. The application of cubic trigonometric B-spline to the numerical solution of the hyperbolic problems. Appl Math Comput 2014; 239: 74-88.

[2] Ay B, Dag I, Gorgulu MZ. Trigonometric quadratic B-spline subdomain Galerkin algorithm for the Burgers' equation. Open Phys 2015; 13: 400-406.

[3] Chang Q, Wang G, Guo B. Conservative scheme for a model of nonlinear dispersive waves and its solitary waves induced by boundary motion. J Comput Phys 1991; 93: 360-375.

[4] Chegini NG, Salaripanah A, Mokhtari R, Isvand D. Numerical solution of the regularized long wave equation using nonpolynomial splines. Nonlinear Dynam 2012; 69: 459-471.

[5] Dag I, Ersoy O, Kacmaz O. The trigonometric cubic B-spline algorithm for Burgers' equation. arXiv:1407.5434, 2014.

[6] Dag I, Saka B, Irk D. Galerkin methods for the numerical solution of the RLW equation using quintic B-splines. J Comput Appl Math 2006; 190: 532-547.

[7] Dogan A. Numerical solution of RLW equation using linear finite elements within Galerkin's method. Appl Math Model 2002; 26: 771-783.

[8] Esen A, Kutluay S. Application of a lumped Galerkin method to the regularized long wave equation. Appl Math Comput 2006; 174: 833-845.

[9] Gardner LRT, Dag I. The boundary-forced regularised long-wave equation. Il Nuovo Cimento B (1971-1996) 1995; 110: 1487-1496.

[10] Hamid NNA, Majid AA, Ismail AIM. Cubic trigonometric B-spline applied to linear two-point boundary value problems of order two. International Journal of Mathematical, Computational, Physical, Electrical and Computer Engineering 2010; 4: 1377-1382.

[11] Hosseini MM, Ghaneai H, Mohyud-Din ST, Usman M. Tri-prong scheme for regularized long wave equation. Journal of the Association of Arab Universities for Basic and Applied Sciences 2016; 20: 68-77.

[12] Irk D. Solitary wave solutions for the regularized long-wave equation. Phys Wave Phenom 2012; 20: 174-183.

[13] Irk D, Keskin P. Cubic trigonometric B-spline Galerkin methods for the regularized long wave equation. Journal of Physics Conference Series 2016; 766: 012032.

[14] Irk D, Keskin P. Quadratic trigonometric B-spline Galerkin methods for the regularized long wave equation. J Appl Anal Comput 2017; 7: 617-631.

[15] Koch PE. Multivariate trigonometric B-splines. J Approx Theory 1988; 54: 162-168.

[16] Lin B. Parametric spline solution of the regularized long wave equation. Appl Math Comput 2014; 243: 358-367.

[17] Lyche T, Winther R. A stable recurrence relation for trigonometric B-splines. J Approx Theory 1979; 25: 266-279.

[18] Mei L, Chen Y. Numerical solution of RLW equation using Galerkin method with extrapolation techniques. Comput Phys Commun 2012; 183: 1609-1616.

[19] Nikolis A. Numerical solutions of ordinary differential equations with quadratic trigonometric Splines. Applied Mathematics E-Notes 2004; 4: 142-149.

[20] Olver PJ. Euler operators and conservation laws of the BBM equation. Math Proc Cambridge 1979; 85: 143-159.

[21] Oruc O, Bulut F, Esen A. Numerical solutions of regularized long wave equation by Haar wavelet method. Mediterr J Math 2016; 13: 3235-3253.

[22] Peregrine DH. Calculations of the development of an undular bore. J Fluid Mech 1966; 25: 321-330.

[23] Saka B, Dag I. A numerical solution of the RLW equation by Galerkin method using quartic B-splines. Commun Numer Meth En 2008; 24: 1339-1361.

[24] Saka B, Dag I, Dogan A. Galerkin method for the numerical solution of the RLW equation using quadratic B-splines. Int J Comput Math 2004; 81: 727-739.

[25] Schoenberg IJ. On trigonometric spline interpolation. J Math Mech 1964; 13: 795-825.

[26] Walz G. Identities for trigonometric B-splines with an application to curve design. BIT 1997; 37: 189-201.

[27] Zaki SI. Solitary waves of the splitted RLW equation. Comput Phys Commun 2001; 138: 80-91.

[28] Zheng K, Hu J. High-order conservative Crank-Nicolson scheme for regularized long wave equation. Adv Differ Equ-Ny 2013; 2013: 287.

[29] Zorsahin Gorgulu M, Dag I, Irk D. Simulations of solitary waves of RLW equation by exponential B-spline Galerkin method. Chinese Phys B 2017; 26: 080202.